Interrelated effects of chromosome size, mechanics, number, location-orientation and polar ejection force on the spindle accuracy: a 3D computational study

Evgenii Kliuchnikov[a], Kenneth A. Marx[a], Alexander Mogilner[b,*], and Valeri Barsegov[a,*]
[a]Department of Chemistry, University of Massachusetts, Lowell, MA 01854; [b]Courant Institute for Mathematical Sciences and Department of Biology, New York University, New York, NY 10012

ABSTRACT **The search-and-capture model of spindle assembly has been a guiding principle for understanding prometaphase for decades. The computational model presented allows one to address two questions: how rapidly the microtubule–kinetochore connections are made, and how accurate these connections are. In most previous numerical simulations, the model geometry was drastically simplified. Using the *CellDynaMo* computational platform, we previously introduced a geometrically and mechanically realistic 3D model of the prometaphase mitotic spindle, and used it to evaluate thermal noise and microtubule kinetics effects on the capture of a single chromosome. Here, we systematically investigate how geometry and mechanics affect a spindle assembly's speed and accuracy, including nuanced distinctions between *merotelic*, *mero-amphitelic*, and *mero-syntelic* chromosomes. We find that softening of the centromere spring improves accuracy for short chromosome arms, but accuracy disappears for long chromosome arms. Initial proximity of chromosomes to one spindle pole makes assembly accuracy worse, while initial chromosome orientation matters less. Chromokinesins, added onto flexible chromosome arms, allow modeling of the polar ejection force, improving a spindle assembly's accuracy for a single chromosome. However, spindle space crowding by multiple chromosomes worsens assembly accuracy. Our simulations suggest that the complex microtubule network of the early spindle is key to rapid and accurate assembly.**

Monitoring Editor
Leah Edelstein-Keshet
University of British Columbia

Received: Nov 14, 2022
Revised: Jan 31, 2023
Accepted: Feb 7, 2023

INTRODUCTION

Before the most dramatic mitotic event—segregation of chromosomes (CHs) in anaphase, the CHs must be integrated into a mitotic spindle during prometaphase (Heald and Khodjakov, 2015). In a proper segregation event, sister kinetochores (KTs) on sister chromatids are attached to microtubules (MTs) amphitelically (O'Connell and Khodjakov, 2007), so that a set of MTs extending from one centrosome (spindle pole) connects with their plus ends to one KT, while another set of MTs from the opposite pole connects to the sister KT (Figure 1E). Several other types of erroneous attachments, most notably *monotelic*, *syntelic*, and *merotelic* (Figure 1E), present problems of various degrees of severity (Cimini and Degrassi, 2005) causing missegregation of the CHs, developmental defects, and diseases (Cimini, 2008; Silk *et al.*, 2013). For example, *monotelic* attachment, in which one KT is connected to one pole, while its sister KT is unconnected (Figure 1E), would not lead the unconnected chromatid to the second pole. In a *syntelic* attachment, both sister KTs are connected to the same pole and are unconnected to the other pole (Figure 1E); as a result, in anaphase both sister chromatids could move to one pole (Figure 1E). *Merotelic* attachment, in which at least one KT is bound to MTs from both poles, could leave the respective chromatid in the middle of the spindle.

This article was published online ahead of print in MBoC in Press (http://www.molbiolcell.org/cgi/doi/10.1091/mbc.E22-11-0507) on February 15, 2023.

*Address correspondence to: Valeri Barsegov (Valeri_Barsegov@uml.edu); Alexander Mogilner (mogilner2@gmail.com).

[AQ 1] Abbreviations used:

© 2023 Kliuchnikov *et al.* This article is distributed by The American Society for Cell Biology under license from the author(s). Two months after publication it is available to the public under an Attribution–Noncommercial-Share Alike 4.0 International Creative Commons License (http://creativecommons.org/licenses/by-nc-sa/4.0).

"ASCB®," "The American Society for Cell Biology®," and "Molecular Biology of the Cell®" are registered trademarks of The American Society for Cell Biology.

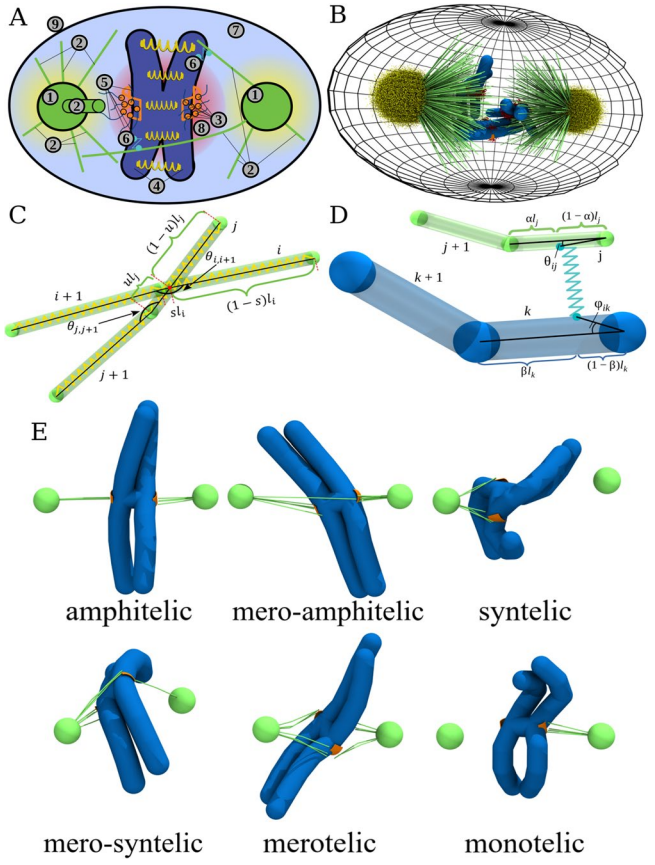

FIGURE 1: Components of the stochastic reaction-diffusion-dynamics model implemented in the *CellDynaMo* package: (A) Schematic of the model. 1) Centrosomes (green); 2) MTs (green); 3) KTs (orange) on which the Ndc80 complexes are bound to MTs with their KT-associated domains are labeled (orange beads); 4) chromosomes (CHs); 5) Ndc80 KT–MT links; 6) chromokinesin (CK) modeled as two harmonically coupled beads with one bead connected to a CH arm and the other bead connected to a MT; 7) blue space is phosphatase (enzyme dephosphorylating Ndc80), which is uniformly distributed in the cell interior; 8) Aurora B kinase (enzyme phosphorylating Ndc80) described by the spherical gradient of its concentration with the central maximum in the space between the KTs (red cloud); and 9) cell boundary (black) is modeled as a repulsive potential for all cell components. Components 1–6 and 9 are described using the Langevin dynamics in the overdamped (Brownian diffusion) limit (see Supplemental Eqs. S14–S17; see also Table 1 and Supplemental Table S2); components 5–8 are modeled using the reaction-diffusion master equation (see Supplemental Eq. S1; see also Supplemental Tables S1 and S2). (B) Snapshot in 3D from the *CellDynaMo*-based simulation that shows all the components. (C) More detailed representation of cylindrical potential (for cylindrical segments of MTs or CH arms) including stretching, bending, and excluded volume interactions between cylinders. Each beginning and end of the cylinder are connected by harmonic springs (shown in yellow). Transparent areas show the excluded volume of each structure. At the intersection point of these volumes, each cylinder is divided into two parts, parametrized by $u \in [0, 1]$ and $s \in [0, 1]$ (see Supplemental Eq. S2). (D) More detailed MT–CH interaction interface. A cylinder-based scheme is used in the *CellDynaMo* force field to model MTs and CH arms. Transparent areas show the excluded volume of each structure. CK is represented as a harmonic potential between two beads on the surfaces of bound cylinders (see Supplemental Eq. S8). Positions of the beads are determined by stochastic chemical reactions and force-velocity relationship (see SM). (E) Types of KT–MT attachments are illustrated by examples coming from snapshots taken from the simulations.

In healthy cells, a missegregating CH is extremely rare—approximately one CH in hundreds of dividing cells, or about 1 out of 10,000 CHs, is missegregated (Santaguida and Amon, 2015). In cancer cell lines and perturbed cells, where the frequency of erroneous connections is much higher than in cells from healthy tissue, tens of percent of attachments are *syntelic* and *merotelic*, transiently (Cimini *et al.*, 2003; Silkworth *et al.*, 2012). However, most of the misattachments are successfully corrected in the cells before anaphase (Cimini *et al.*, 2003, 2006). The attachment error-correction mechanisms are not completely understood, and in this study, we discuss three of them (Gregan *et al.*, 2011; Lampson and Grishchuk, 2017).

The first such mechanism, geometric in nature, prevents the errors rather than corrects those already made: when a *monotelic* connection is made, a pull toward the pole from which the connection is made rotates the CH so that the unconnected sister KT is fully or partially shielded from this pole by the body of the centromere, making a *syntelic* connection less likely (Ostergren, 1951; Gregan *et al.*, 2011; Lampson and Grishchuk, 2017). Similarly, the connected KT is now partially obscured from another pole, making a *merotelic* connection less probable. Note that *monotelic* connections are not errors per se; they just indicate that the spindle assembly is incomplete, and the quantitative question is how much additional time is needed to connect the unattached sister KTs to their proper poles.

The second mechanism is related to correction of *syntelic* errors. Classical experiments by Bruce Nicklas provided direct experimental evidence that KT–MT attachments are stabilized through tension developed across the centromere (Nicklas and Koch, 1969; Nicklas and Ward, 1994; Nicklas, 1997). This suggests the following mechanism of error control (Maresca and Salmon, 2009; Lampson and Cheeseman, 2011; Cane *et al.*, 2013; Krenn and Musacchio, 2015): in *amphitelic* CH attachments, sister KTs are pulled apart, toward the opposite poles, by molecular motors on the MT plus ends. In contrast, with a *syntelic* CH attachment, both sister KTs are pulled in the same direction, toward the same spindle pole, and so there is no stretching between the sister KTs. If there is a way to make MT stability sensitive to the inter-KT stretch, so that the greater the inter-KT stretch, the longer the KT–MT connection's lifetime, then in *syntelic* attachment, MTs will keep detaching from the KTs, until the correct *amphitelic* attachment emerges (Liu *et al.*, 2009). Indeed, multiple experimental studies demonstrated that at early stages of assembly, the number of *syntelic* attachments is large, and then later diminishes to a smaller number close to zero (Cimini *et al.*, 2003; Silkworth *et al.*, 2012). The hypothesized pathway that is likely behind such mechanism is as follows: if Aurora B kinase molecules are tethered to KTs by flexible linkers, their diffusion is limited to a "cloud" around the centromere, like in our model (Figure 1, A and B). Then, stretching between the sister KTs places the KTs outside the Aurora B "cloud." Aurora B phosphorylates long elastic Ndc80 molecular linker regions between the KT and MTs, and as a result of the pull, the Ndc80's phosphorylation level decreases, and the KT–MT attachments become more stable. If, on the other hand, both KTs are kept closer to the center of the Aurora B cloud, as in *syntelic* attachment, then increasing the phosphorylation level of Ndc80 complexes decreases the attachment stability. This mechanism, which we will call *syntelic* correction mechanism for brevity, implies that a soft centromeric spring allowing significant centromere deformation and fast MT turnover would benefit the repair of *syntelic* errors. One of our goals is to test whether this is, indeed, true. Cells typically delay anaphase in the presence of *syntelic* attachments, likely allowing sufficient time for the *syntelic* correction mechanism to work. However, prometaphase in animal cells is relatively fast, from minutes to tens of minutes (Wollman *et al.*, 2005;

Magidson *et al.*, 2011), and so the question is whether this time is sufficient to repair all *syntelic* connections.

Merotelic attachments are more dangerous because anaphase can start before correcting them (Cimini, 2008), and the *syntelic* correction mechanism probably does not work to fix them because *merotelic* MTs do not necessarily negate the centromere stretch. Indeed, existing data suggest that the number of *merotelic* attachments is small, but increases with time during prometaphase (Cimini *et al.*, 2003; Silkworth *et al.*, 2012). One of the hypothesized *merotelic* error-correction pathways is the "brute-force" mechanism: if the number of *merotelic* MTs is much smaller than that of *amphitelic* MTs, then the "wrong" connections could simply be stretched across the spindle (Cimini *et al.*, 2003, 2004) or broken mechanically (Gregan *et al.*, 2011; Gay *et al.*, 2012) in anaphase. Then, the important quantitative question is: what is the expected relative number of *merotelic* MTs?

The search-and-capture model has been a guiding principle for understanding the speed and accuracy of the spindle assembly for decades (Heald and Khodjakov, 2015). According to this model, dynamically unstable MTs grow from the spindle poles, shorten and regrow in random directions, connecting to the KTs by chance (Hill, 1985; Kirschner and Mitchison, 1986; Rieder and Alexander, 1990). In early computational versions of the search-and-capture model, MT attachments to KTs were considered permanent, allowing crude estimates of the speed of the assembly process (Holy and Leibler, 1994; Wollman *et al.*, 2005; Paul *et al.*, 2009; Gopalakrishnan and Govindan, 2011). One of the results of these models was that rapid KT captures are not easily achieved, largely because multiple CHs arms block MT access to many KTs geometrically. Another result was a large number of predicted *merotelic* connections (Paul *et al.*, 2009). Indeed, if all attachments are permanent, then if one waits long enough, many KTs will capture MTs from both poles.

Several years ago, Zaytsev and Grishchuk simulated a single CH and two dynamic MT asters emanating from two spindle poles in 2D, and demonstrated that without geometric error prevention, MT turnover improves the spindle assembly accuracy very little (Zaytsev and Grishchuk, 2015). With geometric error prevention and rapid MT turnover (independent of the centromere stretch in their model), the number of errors can be decreased to a few tens of percent, but the assembly takes a long time. Another notable model in a simplified 3D geometry predicted that a combination of stabilization of KT–MT attachment by centromere stretching, destabilization of misaligned attachments, and hypothetical restriction of a new attachment to an already attached KT to perpendicular MTs only, leads to a very accurate spindle (Edelmaier *et al.*, 2020). Several other recent models addressed these and other aspects of the spindle assembly accuracy (Saka *et al.*, 2015; Tubman *et al.*, 2017; Baudoin *et al.*, 2020; Li *et al.*, 2022).

In our previous study (Kliuchnikov *et al.*, 2022), we revisited the search-and-capture paradigm using the stochastic reaction-diffusion-dynamics model (SRDDM) in conjunction with the *CellDynaMo* computational platform. The SRDDM accounts for 1) molecularly explicit KT–MT connections; 2) kinetics of KT–MT interactions mediated by multiple phosphorylation states of the Ndc80 linkers; 3) diffusing and reacting Aurora B kinase and phosphatase enzymes; and 4) elastic CH arms, MTs, and centromeres. For a single CH, we confirmed earlier results, namely, that there is an optimal rate of MT turnover. We also established that large CH arms slow down CH movements, which has a positive effect on the accuracy, and we found that thermal noise has a complex effect on the accuracy.

In the present study, we made further progress in the SRDDM development and we extended the *CellDynaMo* computational platform, described briefly in *Materials and Methods* and in more detail in the Supplemental Material (SM). These efforts enabled us 1) to systematically explore geometric and mechanical factors affecting accuracy, 2) to consider integration of multiple CHs into the spindle, and 3) to include actions of chromokinesins and polar ejection force (Brouhard and Hunt, 2005; Ye *et al.*, 2016; Almeida and Maiato, 2018). We found that the polar ejection force improves the accuracy by moving the CHs toward the spindle equator, that CH arms limit the effectiveness of the *syntelic* correction mechanism, and that crowding of cellular space is the greatest impediment to the spindle assembly. We also found that truly *merotelic* attachments are predicted to be very rare, which is good news, meaning the reduced CH missegregation rate. [AQ 2]

RESULTS

Classification of the KT–MT connections and geometry of CH positioning

It is useful to make the classification of the KT–MT connections more nuanced, differentiating *merotelic* connections into 1) *mero-amphitelic*, 2) *mero-syntelic*, and 3) simply *merotelic* (Figure 1E; Gregan *et al.*, 2011). This classification is based upon the fact that multiple MTs connect a spindle pole with a KT. First, let us define quantities $L1$ and $L2$ to be the numbers of MTs connecting the left pole (pole 1) and one of the KTs, that is, KT 1 and KT 2, respectively. Similarly, $R1$ and $R2$ are the numbers of MTs growing from the right pole connected to KT 1 and KT 2, respectively. Then, if the total number of MTs connected to KTs is $A1 = L1 + R2$ and the total number of MTs connected to KTs is $A2 = L2 + R1$, then these are two possible types of *amphitelic* attachments. If there are several MTs connecting a KT to pole 1, and only one MT connecting this KT to pole 2, while the sister KT is only connected to pole 2, then this connection is "almost" *amphitelic* (we call it *mero-amphitelic,* if $A1/A2 < 0.25$ or $A1/A2 > 4$). In this case, the majority of MTs stretch the respective centromere, stabilizing the connections, while the single erroneous MT could be broken by overwhelming force from the majority of MTs in later stages of mitosis (Cimini *et al.*, 2003, 2004; Gregan *et al.*, 2011; Gay *et al.*, 2012). Similarly, if several MTs connect one KT to pole 1, several MTs connect the other KT also to pole 1, and very few MTs connect one of the KTs to pole 2, then this connection is "almost" *syntelic* (we call it *mero-syntelic*, if $(L1 + L2)/(R1 + R2) < 0.25$ or $(L1 + L2)/(R1 + R2) > 4$); in this case, the stretch between the sister KTs would be minimal, leading to repair by respective mechanisms. The only truly dangerous connections are purely *merotelic* if at least one of the sister KTs is connected to both poles, and none of the four inequalities above are satisfied.

In all computational case studies reported in this work, we simulate the assembly dynamics for 30 min of biological time, which is one of the longest times measured for prometaphase in animal cells (Wollman *et al.*, 2005). We start with a single CH and investigate how the speed and accuracy of spindle assembly depends on the initial CH position between the poles and orientation. To this end, we test a total of five initial conditions (CH positions and orientations) depicted in Figure 2, A–E. The first three of these initial configurations share the same position at the equatorial plate, shifted by 1.5 μm away from the spindle (pole–pole) axis. The difference between these initial conditions is the initial orientation of the centromere: configuration 1 (Figure 2A) is beneficial for the formation of *amphitelic* attachments, with the centromere (KT–KT) axis parallel to the spindle axis, and sister KTs facing the opposite poles. Configurations 2 and 3 are more "difficult" for proper connections, with the centromere axis being initially perpendicular to the axis of the spindle. In initial

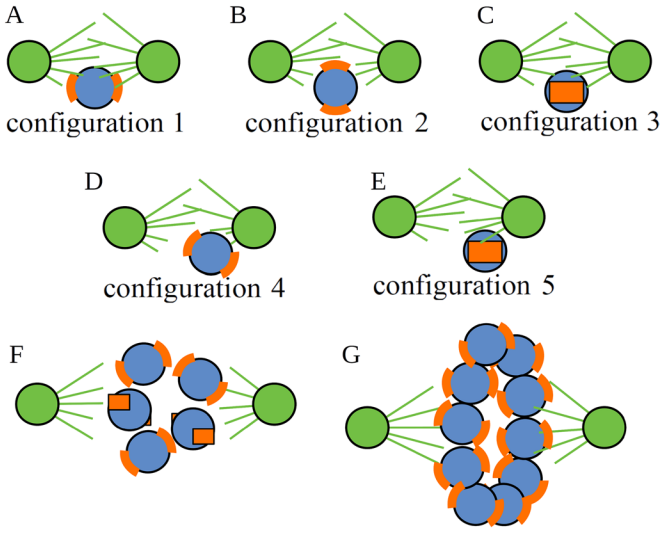

FIGURE 2: Initial cellular positions and orientations of chromosomes used in model simulations. Initial CH position/orientation configurations used in simulations: configuration 1 (A), configuration 2 (B), configuration 3 (C), configuration 4 (D), configuration 5 (E), configuration with multiple CHs placed and oriented randomly (F), and configuration with multiple CHs on a ring in the equatorial plate oriented randomly (G). Orange curved segments show the KT locations. Centrosomes and radiating MTs are indicated in green.

configuration 2, one KT is proximal to the spindle axis and is "visible" equally from both poles, while another KT is shielded from both poles by the centromere body (Figure 2B), which suggests the possibility of formation of more *merotelic* connections. In initial configuration 3, both KTs are equidistant from the spindle axis and are "visible" equally from both poles (Figure 2C), which suggests the possibility of both *merotelic* and *syntelic* connections. In the other two initial configurations 4 and 5, we test how initial asymmetry of chromosome positioning affects the accuracy and the effect of shifting the CH closer to one of the poles (Figure 2, D and E). Here, we try two different initial orientations; in both orientations, however, the centromere axis is perpendicular to the vector connecting the proximal pole to the centromere center. In configuration 4 (Figure 2D), KT 1 is more accessible from the proximal pole, but KT 2 has maximum access to MTs from the distal pole, while KT 1 is almost hidden from the distal pole. In configuration 5 (Figure 2E), both KTs are equally accessible from the proximal pole, and both KTs have equal access to MTs from the distal pole.

Next, we test simultaneous incorporation into the spindle of multiple CHs (Figure 2, F and G). We limit ourselves to simulating a cell with a small number of CHs, say five CHs, like cells of the Indian muntjac, which has just six CHs (Drpic *et al.*, 2018). In one of these tests, the initial positioning and orientations of the CHs are random, but CHs are confined to an imaginary sphere with the poles at two opposite ends of the sphere's diameter (Figure 2F). In another test, following recent findings (Magidson *et al.*, 2011) that in early prometaphase the CHs are located along the equator of the spindle space (imagining that roughly spherical spindle space has "North" and "South" poles where the two centrosomes reside), the CHs are positioned with centromere axes of the CHs oriented in random directions (Figure 2G). These different scenarios of single and multiple CHs to be in different positions and orientations are used in subsequent sections to address the importance of specific factors in spindle assembly accuracy.

Softening of the centromere spring improves spindle assembly's accuracy when CH arms are short, but the effect disappears for long CH arms

To test how centromere deformability affects the connection accuracy, we tested initial configuration 2 (Figure 2B), which is the most susceptible to forming *merotelic* KT–MT attachments, making it hard for the CH to achieve the correct *amphitelic* attachment state. We started with a "naked" CH without CH arms, which is basically a roughly spherical centromere volume with two KTs located on the opposite sides of the volume. Figure 3 (panels E and F) shows examples of erroneous *syntelic* and *mero-syntelic* connections, respectively. We carried out eight independent simulation runs for each of three values of the centromere spring constant, $K_{KT,r}$ = 0.83 pN/nm (soft deformable spring), $K_{KT,r}$ = 83 pN/nm (semiflexible spring), and $K_{KT,r}$ = 333 pN/nm (stiff spring; see Table 2 and Supplemental Eq. S5). The statistics of attachment types shown in Figure 3A indeed illustrates that the softer the spring, the more accurate are the statistics of the attachments: for the soft spring ($K_{KT,r}$ = 0.83 pN/nm), 62.5% attachments are *amphitelic*, with the rest being *mero-amphitelic*, possibly amenable to subsequent correction by brute-force pulling. The stiffer the spring, the lower the number of *amphitelic* attachments, and for stiffer springs, *merotelic*, *syntelic*, and *monotelic* attachments remain after 30 min of biological time (see Table 2). This indicates that the *syntelic* correction mechanism works. For the statistics of attachments, here and below, we counted an attachment as *monotelic* even when the CHs do not have any attachments.

Next, we repeated the simulations for CHs with short (5 μm in length) CH arms (Figure 3G), and found that the difference in the attachment accuracy between the cases with different centromere stiffness remains, with $K_{KT,r}$ = 0.83 pN/nm being best, but then diminishes due to the increased number of *amphitelic* attachments for the cases of semiflexible and stiff springs (Figure 3B and Table 2). The explanation for the improved accuracy is based on consideration of the increased viscous drag of the CH arms: the source of many errors is that the very first attachment pulls (when the attached MT starts shortening, it maintains the connection to the KT and pulls the CH) the CH toward one of the poles, which makes connections from the other pole harder to establish. Analysis of the simulations confirms that bulkier CHs with arms move away from the spindle equator slower, allowing for a longer, more symmetric access of CHs to MTs from both poles (unpublished data). [AQ 3]

Interestingly, when we repeated the simulations for CHs with long (8 μm in length) CH arms (Figure 3G), we found that the difference in the attachment accuracy between the cases with different centromere stiffness has disappeared entirely (Figure 3C and Table 2). The reason is that the CH arms' drag is now so great that it damps the centromeric region movements enough to minimize its deformations. Figure 3D indeed illustrates that the KT–KT stretch of the soft centromere is sufficiently diminished when the CH arms are large. In fact, the softest centromere spring makes the number of *amphitelic* attachments slightly lower than for stiffer springs, probably because the softest spring allows for greatest displacements of the KTs from the equator without the benefit of the error correction, which requires greater centromere stretching. To conclude, the *syntelic* correction mechanism works for shorter CH arms, but not for long CH arms, because the arms' bulk prevents sufficient centromere stretching. However, longer CH arms keep the CHs near the equator, thereby improving the attachment accuracy.

There is an optimal KT size

Several computational studies that used simpler geometries and less detailed models suggested that the assembly speed and accuracy

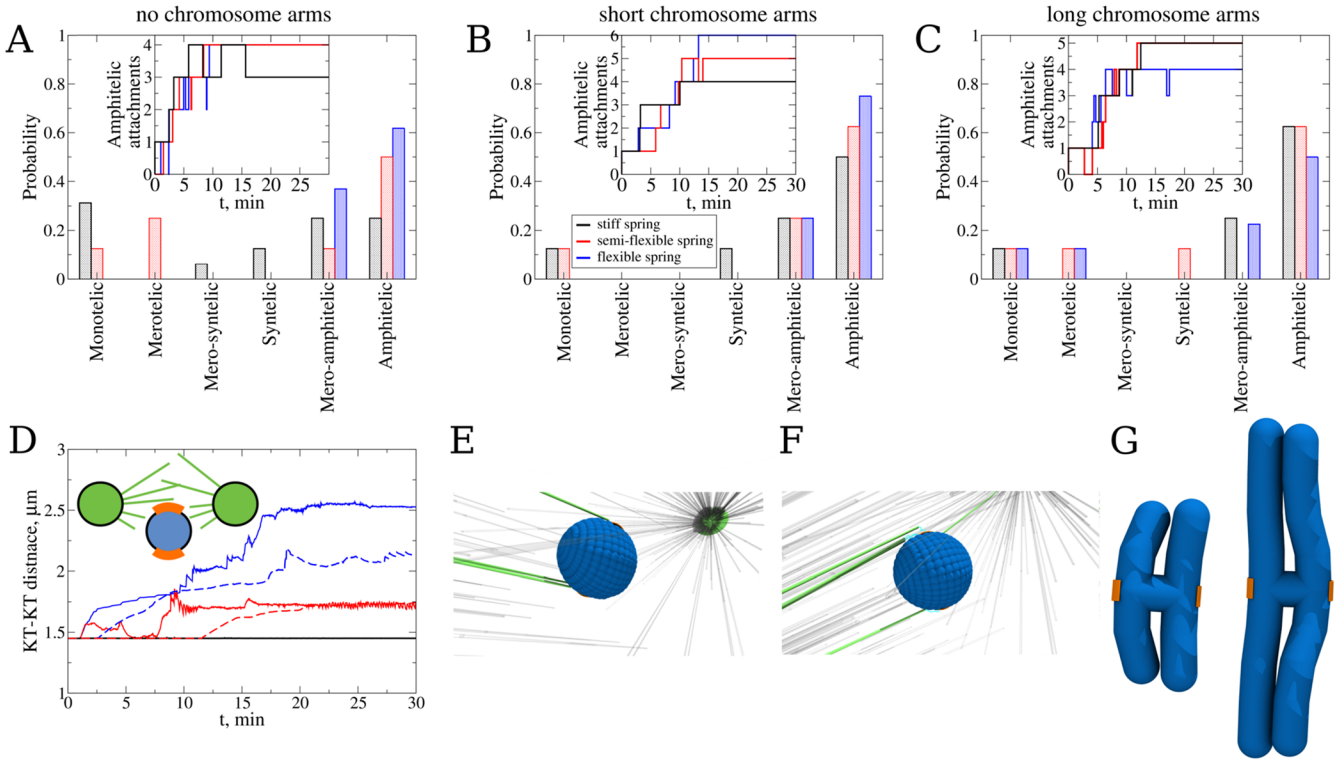

FIGURE 3: Probing the effect of the *syntelic* correction mechanism: (A) Probability to find each type of KT–MT attachments for the system with flexible centromere spring (data shown in blue color) between the sister KTs without chromosome arms, with stiff spring (in black color), and with semiflexible spring (in red color). Probabilities of attachments were determined from attachments collected from eight independent *CellDynaMo* simulations for all three case studies. The total number of *amphitelic* attachments over time collected from all eight simulations for all three case studies are shown in the inset. (B) The same as panel A, but for CHs with short CH arms. (C) The same as panel A, but for CHs with long CH arms. (D) Separation distance between the sister KTs as a function of time for the most representative simulation run for the systems with flexible (blue), semiflexible (red), and stiff centromere spring (black). Solid lines show the time series for the case with KTs without CH arms, and dashed lines show the time series for the case with CH arms. (E) Example of *syntelic* attachment. (F) Example of *mero-syntelic* attachment. Centrosomes are shown as green beads, the blue corrugated ball is the centromere, KTs are shown in orange, unconnected MTs are displayed in gray, connected MTs are shown in green, and cyan links are Ndc80 complexes. (G) Comparison of CHs with short and long CH arms.

impose conflicting requirements on the KT size: a small KT presents a small target for the searching MTs and requires a longer time to capture, but a large KT can be more easily captured from the opposite poles, thereby creating errors. To confirm that there is an optimal KT size for the spindle assembly, we simulated a "naked" CH in initial configuration 2 (Figure 2B), with the soft centromere spring constant ($K_{KT,r}$ = 0.83 pN/nm). We varied the surface area of the curved KT from A_{KT} = 0.03 µm^2 (small KT) to A_{KT} = 0.15 µm^2 (intermediate KT), and to A_{KT} = 0.36 µm^2 (large KT). The statistics of KT–MT attachments shown in Figure 4A confirms the intuition: in the large KT case, just 25% of all attachments are *amphitelic*, while the majority of the attachments are *mero-amphitelic*. An example of *merotelic* connections made in this case is shown in Figure 4D (see Table 2).

KTs with the smallest surface area A_{KT} = 0.03 µm^2 did not result in a single *amphitelic* attachment; most attachments were *monotelic*. Inspection of the simulations shows that it is so difficult to capture such a small KT, so that a rare single attachment would lead to eventual pulling of the CH toward the pole from which the capture is made. During the time of the pull, the probability to capture the sister KT is too small, and after the CH is pulled to one of the poles, this probability is even smaller, due to the increased distance to the other pole with the decreased solid angle subtended by the KT array for MT searching and capture. The intermediate KT area (A_{KT} = 0.15 µm^2) resulted in 62.5% *amphitelic* attachments, suggesting that this value is close to the optimal KT size, resulting in a compromise between the speed and accuracy of attachment. In all simulations described below (including the simulations described in the previous section), we used this optimal intermediate KT surface area of A_{KT} = 0.15 µm^2 (see Table 2).

Initial proximity to one spindle pole makes the accuracy of the spindle assembly worse

Another geometric factor affecting attachment accuracy is the initial position and orientation of the CH with respect to the spindle poles. To evaluate this factor, we carried out eight independent simulation runs for each initial configuration 1–5 (Figure 2, A–E). The statistics of resulting attachments summarized in Figure 4B confirm intuitive expectations. First, there are 100% *amphitelic* attachments for initial configuration 1 (Figure 2A), in which sister KTs face the opposite poles, are equally close to them, and are shielded by the centromere body from the other pole they are not facing. In the same initial position, changing the initial orientation of the centromere worsens the attachment accuracy, but not dramatically so. Starting from initial configurations 2 and 3 (Figure 2, B and C), about 60% of

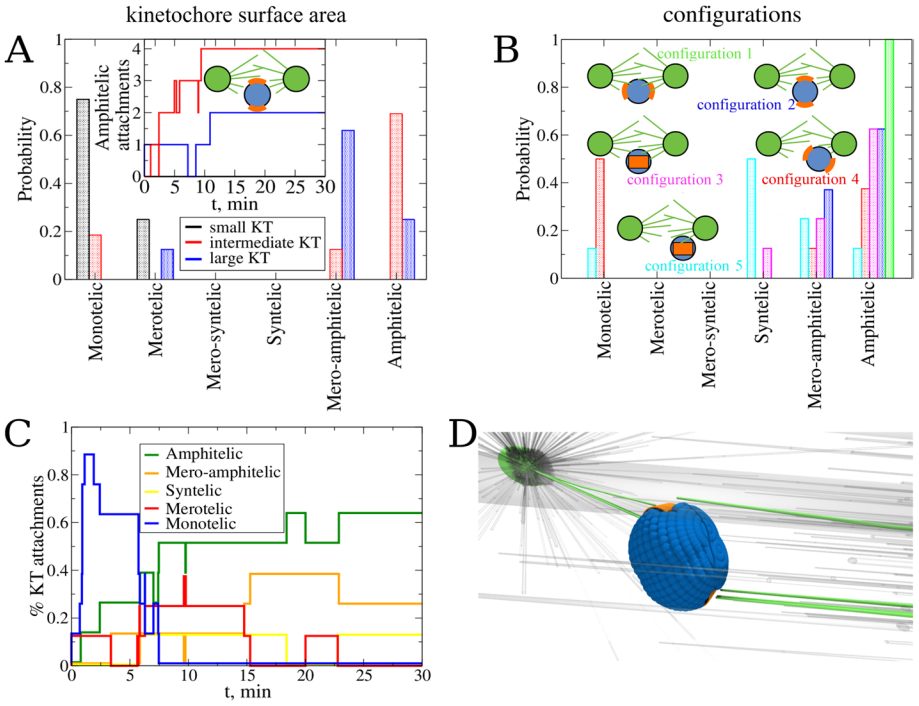

FIGURE 4: Exploring the effect of the kinetochore size and initial configuration of the chromosome. Panels A and B show the effect of the KT surface area on the attachment accuracy. (A) Probability to find each type of attachment for the system with large (blue), intermediate (red), and small (black) KT surface area. Statistics of attachments were collected from eight independent *CellDynaMo* simulations for all three case studies. The number of *amphitelic* attachments as a function of time collected from all eight simulation runs for all three case studies are shown in the inset. (B) Probability to find each type of attachment for the system with a single KT pair without CH arms. Different colors represent different initial positions and orientations (see Figure 2, A–E): configuration 1 is green, 2 is blue, 3 is magenta, 4 is red, and 5 is cyan. Statistics were collected from eight independent simulations for all initial configurations 1–5. (C) The normalized number of attachments of different types as a function of time collected from all eight simulation runs for initial configuration 3. (D) Snapshot of a final position and orientation for the largest KT surface (*merotelic* attachment).

amphitelic connections emerge, with almost all the rest being *mero-amphitelic* attachments that could be corrected later by the brute-force mechanism. The only exception is the very small percentage of *syntelic* attachments emerging from the initial configuration 3 (Figure 2C), which is not unexpected because such an initial orientation has both sister KTs equally accessible from the same pole. As expected, many *monotelic* connections are made rapidly, within the first few minutes, and then as rapidly the number of such connections decreases (Figure 4C). We see that the numbers of *syntelic*, *amphitelic*, and *mero-amphitelic* attachments roughly increase in the first 10 min and then stabilize (Figure 4C).

Initially placing the CH close to one of the poles makes the attachment accuracy significantly worse, as initial configurations 4 and 5 (Figure 2, D and E) demonstrate. Many *syntelic* connections arise from initial configuration 5, as expected, because both KTs are equally accessible from the proximal pole, while being too far from the distal pole. No *syntelic* and many *monotelic* connections emerge from initial configuration 4. Inspection of the simulations indicates the reason, which is that one of the KTs now has large access from the proximal pole, while its sister KT is too far from the distal pole. This secures many attachments to the former KT locking the CH in the *monotelic* orientation. The overall conclusion from this study is that initial asymmetry of the CH positioning poses a great challenge for the accuracy of attachment, while the initial CH orientation matters less.

Crowding of the spindle space by multiple CHs makes the spindle assembly accuracy worse

Now that we have understood how a single CH is incorporated into the spindle, we next turned to describing multiple CHs undergoing interactions with MTs simultaneously, but still for the case of naked CHs without arms. To this end, we performed 10 independent simulations for the system with five CHs, initially randomly placed and randomly oriented within the sphere of 2.5-μm radius (Figure 5, A and D). Final spindle configurations are shown in Figure 5, B and E, and the statistics of attachments are shown in Figure 5C. We see that after 30 min of biological time, only 25% of attachments are *amphitelic*, with an almost equal percentage of *syntelic* attachments and 50% *monotelic* attachments. Inspection of the simulations shows that some of the CHs that are initially close to one of the poles become *monotelic*, as our previous case study showed; then, these CHs block many MTs from accessing the equatorial region of the spindle, thereby hindering the formation of *amphitelic* attachments. Some of the CHs that are very close to one of the poles, expectedly, form *syntelic* attachments.

Next, we carried out similar numerical experiments, but now for 10 naked CHs. Based on previous experimental observations suggesting that in early prometaphase the CHs are crowded to the ring-like region around the spindle equator (Magidson *et al.*, 2011), we placed the CHs into such a ring and randomized the initial orientations of the centromere axes (Figure 5F). A total of 10 simulation runs for each of the random initial orientation set resulted in the statistics of attachments shown in Figure 5H; one of the final configurations is shown in Figure 5G. We see that, compared with the random initial positioning of multiple CHs, there is a significant accuracy improvement for CHs positioned in the ring-like region: the number of *amphitelic* attachments increases, and the numbers of *syntelic* and *monotelic* attachments decreases, confirming the previous result that initial equatorial positioning is the most important accuracy booster. However, the accuracy for the multiple CHs initially placed at the equator is worse than that for a single CH placed at the equator, and is comparable to that for a single CH initially placed near one of the poles. Inspection of the simulations shows that the reason is like that for the initial random CH positioning: just a few CHs pulled to the poles shield many remaining CHs from the MTs, thereby hindering new connections and also blocking each other's access to MTs from the distal poles, which could subsequently improve the attachment accuracy.

Polar ejection force improves spindle assembly accuracy for a single CH

After having addressed the question of which geometric and mechanical factors affect the accuracy of the spindle assembly, we

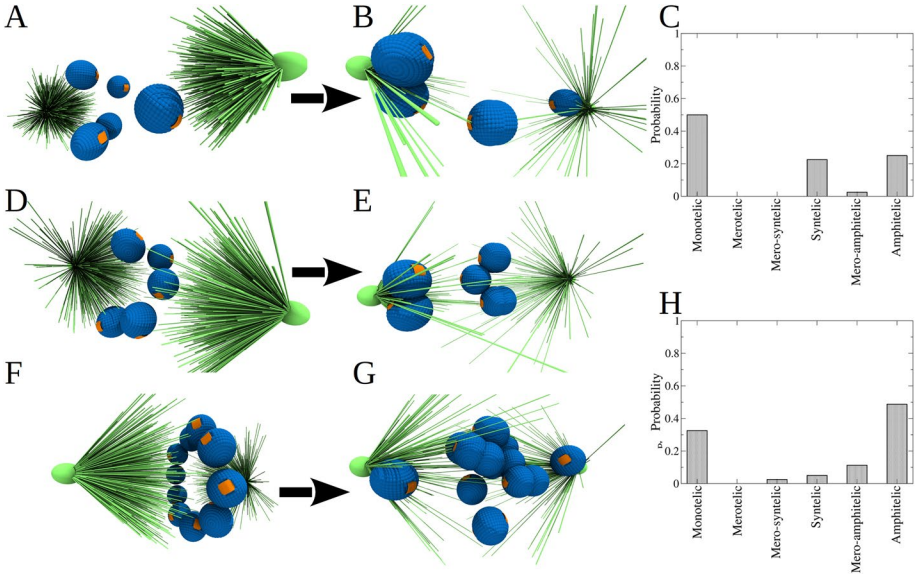

FIGURE 5: Assembly accuracy for the case of multiple "naked" CHs. (A, D) Initial frames of two examples of the system with 5 KT pairs randomly distributed and oriented. (B, E) Final frames (30 min of cell dynamics) of the systems shown in panels A and D, respectively. (C) Probability to find each type of KT–MT attachments for the system with 5 KT pairs randomly distributed. Statistics of attachments were collected from 10 independent *CellDynaMo* simulation runs. Snapshot for the initial configuration, where four out of five KT pairs have access to MTs from both CSs. (F) Snapshot of the initial configuration of the system, in which 10 KT pairs are placed in the equatorial plate forming a ring; the initial orientation of each KT pair is random. (G) Snapshot of the system with 10 KT pairs after 30 min of cell dynamics. (H) Probability to find each type of KT–MT attachments for the system with 10 KT pairs. Statistics of attachments were collected from 10 independent simulation runs.

turned to the case of CHs with CH arms present (8 μm in length), starting with a single CH with deformable cylindrical arms placed in initial configurations 1, 2, and 4 (Figure 2, A, B, and D respectively). The statistics of attachments are shown in Figure 6A. Similar to the behavior of the naked CH, initial configuration 1 resulted in 100% *amphitelic* attachments. Initial configuration 2 resulted in slightly worse statistics than the same initial configuration for the naked CH in the sense that the number of *amphitelic* attachments decreased while the number of *mero-amphitelic* attachments increased. Inspection of the simulations shows that the reason is that the CH arms slow down CH turning after the very first attachment is made, allowing time for multiple attachments to the same KT from the opposite poles to form. Initial configuration 4 led to roughly similar attachment accuracy to that of the naked CH case.

These results show that the mere presence of the CH arms does not improve the attachment accuracy, despite the expectation that growing MTs push on the CH arms and, therefore, generate the so-called polar ejection force pushing the CHs away from the poles into the equatorial region of the spindle, where the average MT numbers from both poles equalize and the net push from the poles balances. In fact, we found in our previous computational study that this expectation fails because the growing MTs slip off the CH arms' surface, bend slightly and keep growing, therefore not generating the polar ejection force (Kliuchnikov *et al.*, 2022). Thus, as simulations illustrate, a CH that is located near one of the poles by KT–MT connections to this pole, has its CH arms more or less straight indicating the negligible polar ejection force in this case (Figure 6C).

To further investigate the effect of polar ejection force, we added chromokinesin (CK) motors to the CH arms (Almeida and Maiato, 2018), so that the MTs that have lateral contacts with the CH arms provide tracks for the CK motors that move to the MT plus ends and generate the pushing forces (see Supplemental Eq. S8). Evidence that there is such a net polar ejection force is seen in Figure 6D, where the CH arms are bent away from the proximal pole. We found, though, that such forces are not sufficient to move the whole CH to the spindle equator (Figure 6D), because even when a CH is close to one of the poles, many MTs are captured by the KT proximal to the pole. Taken together, all such MTs generate pulling forces that overwhelm the polar ejection force. In this case, when the CH starts moving from initial configuration 2, there is little change in the attachment statistics (Figure 6B), which is not surprising because the CH starts off near the equator, where the ejection forces from both poles balance. When the CH starts off from initial configuration 4, CKs help improve the percentage of the *amphitelic* attachments, but they also increase the percentage of the *syntelic* attachments (Figure 6D), indicating that many CHs remain near the initially proximal pole. This is shown in Supplemental Movie S1. Examples of final CH states predicted by these simulations are shown in Figure 6, F and G. Note the CH arms are being pushed away from the cloud of the spindle MTs by the polar ejection forces. These V shapes of the CH arms resemble the experimentally observed CH arms' shapes (see Supplemental Movie S1).

When, in addition to the existence of CKs on the CH arms, we limited the number of MTs that can connect to a KT (see *Dynamics of microtubules—interactions with chromosomes* in the SM), the attachment accuracy for the "worst" initial configuration 4 improved dramatically, as displayed in Figure 6B, with more than 70% *amphitelic* attachments formed. Note the characteristic position of the CH in Figure 6E that now is being pushed away from the pole significantly by the action of CKs. This positioning of the CH to the equatorial region significantly improves the probability of achieving *amphitelic* attachments. The still relatively high percentage of *syntelic* attachments likely can be repaired by error-correction mechanisms. Note also that before these simulations, the best we could achieve with *monotelic* attachments was to bring their numbers down to 10%. Now, the polar ejection force helps to keep the number of *monotelic* attachments around zero, even for the "worst" initial configuration 4. This is shown in Supplemental Movie S2.

Crowding effect largely cancels the effect of the polar ejection force

Finally, we carried out eight independent simulations for a system with five CHs with CH arms, CK action, and a limited number of allowable KT–MT attachments. In these simulations, the CHs were initially placed in random initial positions and orientations (see Figure 7A). The characteristic final configuration of the CHs is shown in Figure 7B. Note that now there are no CHs falling onto the poles because of the polar ejection force. Nevertheless, the attachment statistics shown in Figure 7C demonstrate that the accuracy remains low: just 25% of all CHs achieve *amphitelic* attachments by the end of the 30-min simulations, while more than 40% of all CHs end up

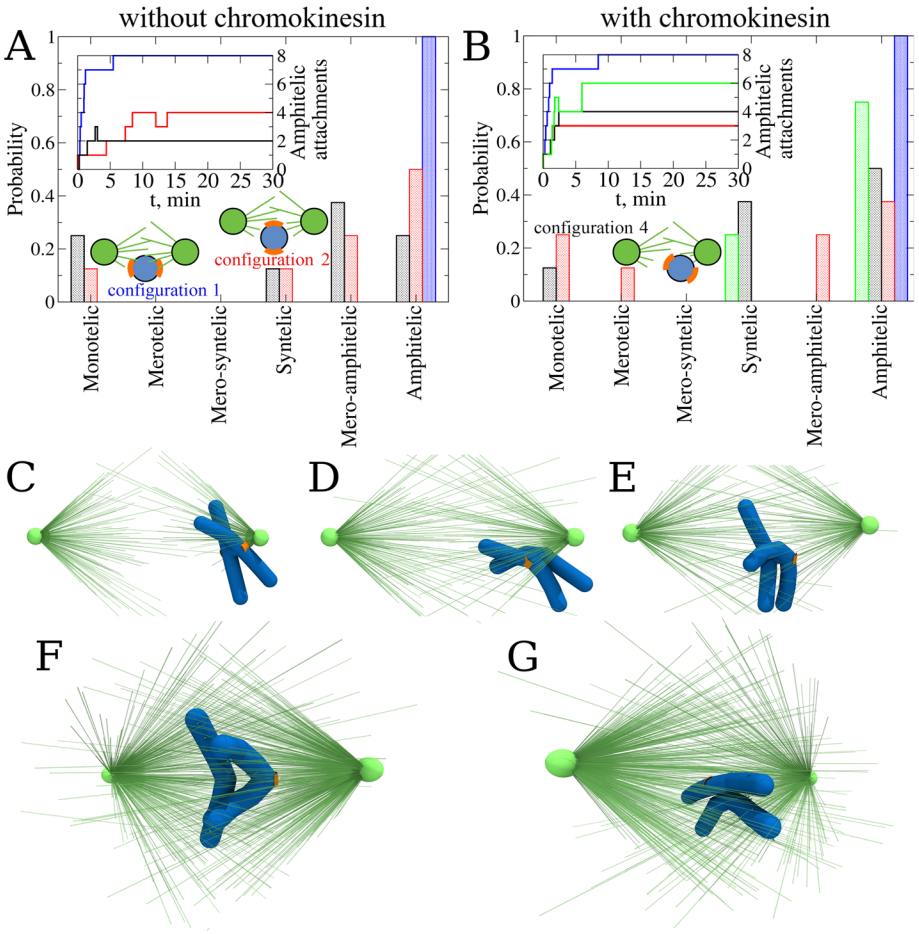

FIGURE 6: Probing the role of chromokinesin and polar wind. (A) Probability to find each type of KT–MT attachments for CHs without chromokinesins (CKs) in different initial configurations: 1 (blue), 2 (red), and 4 (black). Statistics of attachments were collected from eight independent *CellDynaMo* simulations for all three case studies. The number of *amphitelic* attachments as a function of time collected from all eight *CellDynaMo* simulation runs for all three case studies are shown in the inset. (B) Probability to find each type of KT–MT attachments for CHs in the presence of CK in different initial configurations: 1 (blue), 2 (red), and 4 (black). Green bars correspond to the case of CH in initial configuration 4, but with a limited number of MTs allowed to attach to the KTs. Statistics were collected from eight independent *CellDynaMo* simulation runs for all three case studies. The number of *amphitelic* attachments as a function of time collected from all eight trajectories for all three case studies are shown in the inset. (C) The most representative snapshot of the final position of CH (after 30 min of simulation) for the case without CK. (D) The most representative snapshot of the final position of CH (after 30 min of simulation) for the case with CKs and an unlimited number of MTs allowed to attach to the KTs (see Supplemental Movie S1). (E) The most representative snapshot of the final position of CH (after 30 min of simulation) for the case with CKs and a limited number of MTs allowed to attach to the KTs (see Supplemental Movie S2). (F) Snapshot of the final position and orientation for *amphitelic* attachment. (G) Snapshot of the final position and final orientation for *merotelic* attachment.

forming *monotelic* attachments. Thus, the crowding and resulting shielding of many KTs from the poles reduce the likelihood of formation of proper attachments, even in the presence of the polar ejection force and better biasing of the CHs to the equator. This is illustrated in Supplemental Movie S3. The good news, though, is that there are no *merotelic* connections as predicted for the multiple CH system (Figures 5 and 7), probably because the crowding also protects KTs from the access to MTs from both poles. Note that the attachment statistics of this final case study is slightly better than that for multiple naked, initially randomly placed CHs (Figure 5C). The CH arms make the crowding worse, so without CKs and polar ejection force, the statistics are expected to be worse. Lastly, the time series for the attachment numbers (Figure 7C) show that the majority of *monotelic* connections are made between the first 5 and 10 min of simulations, that is, much later than in the case of a single CH (Figure 4C). After 10 min of the search, the *monotelic* connections are converted slowly but steadily into the *syntelic*, *mero-amphitelic*, *and amphitelic* connections; yet, the conversion is not complete. Note also a small transient number of *merotelic* connections. To conclude, the polar ejection force improves the accuracy of the spindle assembly, but crowding largely counteracts and cancels this improvement.

DISCUSSION

Extension of 3D search-and-capture model

We developed the extension of the mechanochemical 3D SRDDM of the search-and-capture pathway of mitotic spindle assembly (Kliuchnikov *et al.*, 2022) implemented in the *CellDynaMo* package. To make the dynamics of interactions between the cell components more realistic, that is, to model accurately excluded volume interactions, we implemented the cylindrical potential to the model (Figure 1C and Supplemental Eqs. S2 and S9). This made it possible to model molecular motors, such as CK motors, walking on MTs (Figure 1D and Supplemental Eqs. S8 and S13). The advantage of this approach, over the previous work (Kliuchnikov *et al.*, 2022), is that one can now computationally describe more complex processes, such as the polar ejection force. This extension will enable us to explore in future studies the formation of the spindle interpolar bundles (via adding kinesin-5 to the model; Peterman and Scholey, 2009), and to describe the KT–MT interface by adding dynein to the model (Vaisberg *et al.*, 1993).

Model's implications for the accuracy of CH integration into the spindle

The *CellDynaMo*-based simulations we have performed, satisfyingly, confirm that the more deformable the centromere, the more accurate the assembly. The intuitive explanation is the following: the *amphitelic* attachments, associated with greater centromere stretch, move CHs away from the Aurora B cloud, and resulting biochemical pathways solidify this attachment type. *Syntelic* attachments lack the centromere stretching, keeping the sister KTs close to each other and inside the Aurora B cloud, which leads to destabilizing the KT–MT connections in these attachments. The nontrivial prediction from our study is that this effect is largely canceled by bulky CH arms; the same accuracy is achieved with stiff and soft centromeres if the arms are large. The

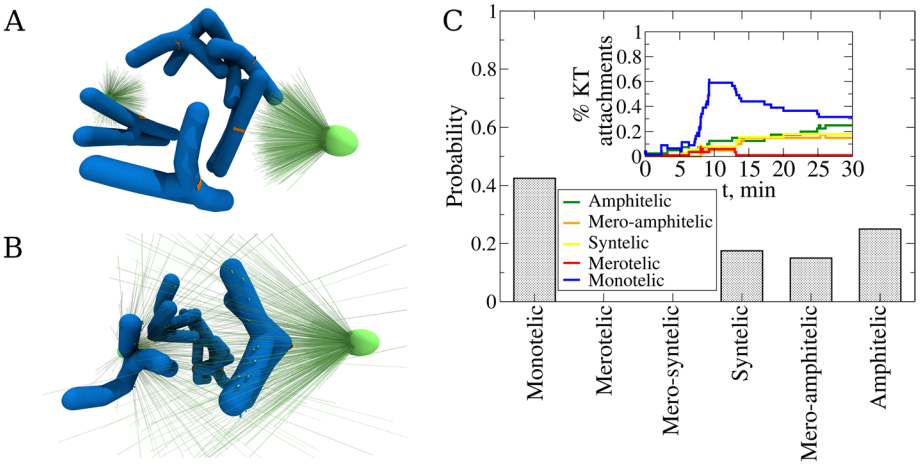

FIGURE 7: Exploring cell dynamics with multiple chromosomes in the presence of chromokinesin. (A) Snapshot of a random initial configuration of the spindle. (B) Snapshot of the final spindle configuration after 30 min of *CellDynaMo* simulation (see Supplemental Movie S3). (C) Probability to find each type of attachment from eight independent *CellDynaMo* simulation runs. The normalized number of attachments of different types as a function of time collected for all 40 chromosomes (5 chromosomes times 8 simulation runs) is shown in the inset. Color denotation is shown in the graph.

reason is that a great viscous drag on the CH arms makes fast KT displacements and KT turns less likely, thereby negating the elastic deformations of the centromere, and preventing disastrous events of CHs collapsing onto the poles.

The SRDDM also demonstrates that the key for high attachment accuracy is keeping CHs near the equator: when a CH gets too close to one of the poles, the very likely outcome is a *monotelic* connection. The sister KT, while facing away from the proximal pole, is then too far from the distal pole to capture any of its growing MTs. The *CellDynaMo* simulations show that one possible strategy to improve the attachment accuracy is to initially position the CHs along the equator (Magidson *et al.*, 2011), while another is to harness the polar ejection force generated by CKs to repel the CHs from the poles. For the latter, it is crucial to limit the number of MTs allowed to connect to a KT, so that the pulling force on the KT does not overwhelm the pushing force on the KT arms. Interestingly, the initial orientation of the CH matters less, likely because multiple pulls and pushes randomize the orientation before a significant number of attachments has been established.

The results of *CellDynaMo* simulations show that space crowding by CHs with large CH arms has the greatest deleterious effect on achieving proper and fast CH attachments, mainly because CHs block access of many KTs to MTs from the spindle poles. The signature of the crowded space for the spindle is a very high percentage of *monotelic* attachments, in which many KTs do not capture any MTs. In this study, we only simulated the spindles with a small number of CHs, and so, clearly, the simulations with a greater CH count would show even more dismal accuracy statistics.

Nevertheless, the good news is that *monotelic* attachments are not erroneous per se; they are the sign that the assembly goes slowly, and that there needs to be a way to accelerate the KT–MT access (as discussed below). Our simulations with multiple CHs often showed no *merotelic* attachments, which are the most dangerous of all incorrect attachments. Curiously, there were no *mero-syntelic* attachments formed in our computational experiments. The moderate numbers of *syntelic* attachments predicted in our simulations likely mean that more effective error-correction mechanism(s), capable of discriminating between the low- and high-tension states of the centromere, are missing from the model. Moderate numbers of predicted *mero-amphitelic* attachments could be corrected with the "brute-force" mechanism.

Additional comments on model parameters

In this article and in our earlier study (Kliuchnikov *et al.*, 2022), we investigated how the speed and accuracy of the spindle assembly depend on key parameters, including (but not limited to) MT turnover time, KT size, centromere stiffness and CH initial position and orientation. Inevitably, current computational and presentational limitations precluded us from varying some important parameters. Here we make brief qualitative comments on several such model parameters. We have not varied the shape or volume of the cellular space or scaled them with the CH arms' shape or volume. Intuitively, a larger cellular space relieves crowding, but also leads to fewer searching MTs per CH (Wollman *et al.*, 2005), so it may be expected that there is an optimal complex scaling between the CH count and volume, cell volume, and number of MTs. Investigating such an optimum in the presence of a realistic MT network is an important problem for future studies. One of the important effects of the CH size is the slowing down of shifts and turns of the CHs. This effect seems to become noticeable from a few microns' length of a CH. CH arms' flexibility is another interesting parameter. Arms that are too stiff will likely hinder necessary CH movements in the crowded space, while arms that are too flexible will stop slowing centromeres down and diminish the effect of the polar ejection force. Lastly, motor forces have to be balanced in the spindle; in our case, this means that we chose the CK force, the number of these motors per CH, and the upper limit on the KT–MT connections so that the net effective poleward force is roughly equal to the net polar ejection force per CH. Significant (order of magnitude) shifts of this balance in either direction worsens the assembly accuracy.

What is missing in the current model

Crowding of the spindle space by the CHs is inevitable, and the likeliest mechanism to avoid the exceedingly slow formation of connections in the crowded space is for the spindle to deploy an MT network more complex and dynamic than that emanating solely from two centrosomal asters. Indeed, a recent study suggests that initially indiscriminate connections between short MTs, preconnected to or growing from KTs, and long centrosomal MTs improve the accuracy of the spindle assembly drastically, due to an action of dynein motors sorting out transient incorrect connections (Renda *et al.*, 2022). It remains to be seen what the predictions of a 3D model with multiple CHs for such KT–MT-dynein motor arrays will be, but clearly future models will have to include more motor types than just CKs. MT branching can also potentially fill the space much more efficiently with MT plus ends (Thawani *et al.*, 2019). Rapid MT pivoting is yet another mechanism that can accelerate the KT capture (Kalinina *et al.*, 2013; Blackwell *et al.*, 2017). Keeping CHs in the equatorial plane of the spindle is another important factor predicted

Model component	Component type	Functional role
Chromosome (CH)	Mechanical	Flexible genomic DNA-nucleoprotein packages segregating during mitosis
Kinetochore (KT) corona	Mechanical	Interactions with growing and shortening MTs through the plus-ends attachment
Centrosome (CS)	Mechanical	Microtubule organizing center
Microtubule (MT)	Mechanical/Chemical	Pushing and pulling forces acting on CHs through MT plus-end growth and shortening
Ndc80 linker	Mechanical/Chemical	Formation and disruption of noncovalent linkages between MT plus end and KT corona
Chromokinesin (CK) motor	Mechanical/Chemical	Formation of the reversible linkages between a MT and a CH arm
Aurora B kinase	Chemical	Phosphorylation of Ndc80 linkers
Phosphatase	Chemical	Dephosphorylation of Ndc80 linkers
Cohesin rings	Mechanical	CH arms constraining
Cell membrane	Mechanical	Delineation of the interior space of the cell

TABLE 1: Components of stochastic reaction-diffusion-dynamics model: list of components of the SRDDM along with their component type and functional role, including chromosomes (CHs), their sister kinetochores (KTs), centrosomes (spindle poles), microtubules (MTs), Ndc80 protein linkers anchored at the KTs, chromokinesin (CK) motors, Aurora B kinase, phosphatase kinase, cohesin rings, and cell membrane (see Figure 1 for graphical illustration; see also Supplemental Tables S1 and S2 for more detailed information for each component).

(Magidson *et al.*, 2011). One of the elegant ways that this can be achieved is for the spindle poles to segregate from each other rapidly and symmetrically, simply leaving the crowd of CHs at what will become the spindle equator (Magidson *et al.*, 2011). Inclusion of the interpolar MT bundles (Nédélec, 2002) and interactions of the astral MTs with the cell cortex (Farhadifar *et al.*, 2020), responsible for the pole–pole segregation, will also have to be included in the next-generation computational models. Other molecular mechanisms, potentially improving the accuracy of mitosis, include the dynamic "lock" that selectively and rapidly stabilizes proper end-on attachments (Conti *et al.*, 2019), dynamic KT shapes (Magidson *et al.*, 2015), KT behaving as a tension-sensitive catch bond (Akiyoshi *et al.*, 2010), and regulation of MT dynamics by Ran protein (Pavin and Tolić, 2016).

Why model the search and capture at all?

In the last few years, it became clear that the original search-and-capture model was not describing well enough the spindle assembly process (O'Connell and Khodjakov, 2007; Meunier and Vernos, 2016; Letort *et al.*, 2019; Renda *et al.*, 2022). Most notably, the majority of the initial contacts between the long centrosomal MTs and KTs are lateral (Magidson *et al.*, 2011), not end-on attachments, and short MTs (Sikirzhytski *et al.*, 2018) actively mediate connections formed between the KTs and long centrosomal MTs. Why then, explore the search-and-capture model further? There are three main reasons. First, design principles of the spindle assembly become clearer as a result. Second, like in machine engineering, it is likely that the cell uses redundant mechanisms (of which the search-and-capture is one) to achieve higher accuracy (Bentovim *et al.*, 2017). Lastly, other unrelated cell biological phenomena also harness elements of the search-and-capture process (Lee *et al.*, 2000; Gundersen, 2002; Drake and Vavylonis, 2010; Vinogradova *et al.*, 2012; Sarkar *et al.*, 2019).

[AQ 4] ## CONCLUSION

XXX

MATERIALS AND METHODS

[AQ 5] Request a protocol through *Bio-protocol*.

Model components

The SRDDM, implemented in the *CellDynaMo* package (Kliuchnikov *et al.*, 2022) is described in detail in the SM and is graphically summarized in Figure 1. Briefly, the SRDDM model includes the *mechanically active* components, which participate in the mechanical processes (e.g., chromosome pulling and pushing, stretching and bending of chromosome arms, mechanical coupling between microtubules and kinetochores; see Supplemental Eqs. S2–S10), and the *chemically active* components, which interact in the chemical reactions (e.g., phosphorylation by Aurora B and dephosphorylation by phosphatase, microtubule polymerization and depolymerization, formation and dissociation of linkages between microtubules and kinetochores, attachment and detachment of chromokinesins). In addition, several components are *active both mechanically and chemically*, which builds the mechanochemistry into the model. For example, microtubule polymerization and depolymerization (chemistry) results in pushing and pulling forces exerted on chromosomes (mechanics; see Table 1, and Supplemental Tables S1 and S2). In SRDDM, the volume of the cell is constant in all simulations, and it does not scale with the CH number.

Mechanical components

The SRDDM model involves the following *mechanically active* components: centrosomes (spindle poles), MTs, sister KT pairs on the centromeric regions of CHs, Ndc80 protein linkers anchored at the KTs, and CK motors (Table 1 and Figure 1; see also Supplemental Tables S1 and S2). The time evolution of all the mechanical components is described using the Langevin dynamics (LD) in the Brownian diffusion limit (see SM). The MTs are elastic filaments. The model also includes centromeres ("naked CHs") described as spherical beads (the *sister KT pair* is described by a pair of beads connected by a harmonic spring); these centromeres can be modeled with or without the CH arms. Sister chromatids, CH arms, are described as elastic cylinders. The model also mimics the constraints on CH arms due to cohesin rings; the CH ends can swing away from each other, within limits. The KTs are described as a dense grid of small spherical particles connected by elastic springs that lie on the spherical bead surface of centromeres (see Supplemental Eq. S5). The Ndc80 proteins are represented by elastic springs attached to the KT

Figure	Case study	Varied model parameters		
		Parameter	Value	Findings
3	No chromosome arms	$K_{KT,r}$	0.83 pN/nm	62.5% *amphitelic*, 0% *merotelic*
			83.0 pN/nm	50% *amphitelic*, 25% *merotelic*
			333.0 pN/nm	25% *amphitelic*, 0% *merotelic*
	Short chromosome arms (5 μm)	$K_{KT,r}$	0.83 pN/nm	75% *amphitelic*, 0% *merotelic*
			83.0 pN/nm	62.5% *amphitelic*, 0% *merotelic*
			333.0 pN/nm	50% *amphitelic*, 0% *merotelic*
	Long chromosome arms (8 μm)	$K_{KT,r}$	0.83 pN/nm	50% *amphitelic*, 12.5% *merotelic*
			83.0 pN/nm	62.5% *amphitelic*,12.5% *merotelic*
			333.0 pN/nm	62.5% *amphitelic*, 0% *merotelic*
4	Kinetochore surface area	A_{KT}	0.03 μm^2	25% *amphitelic*, 12.5% *merotelic*
			0.15 μm^2	65% *amphitelic*, 0% *merotelic*
			0.36 μm^2	0% *amphitelic*, 25% *merotelic*

TABLE 2: Parameters varied in stochastic reaction-diffusion-dynamics model: numerical values of SRDDM parameters, which were varied and the simulation output. The most optimal findings are highlighted as bold.

surface that can form the reversible linkages with MTs (Supplemental Eq. S5). The rate of Ndc80 detachment from an MT, and thus the KT–MT connection's stability, depends on the Ndc80 phosphorylation state, as explained in the SM. When an MT bumps into a KT, Ndc80 can form a linkage between the plus end of a growing MT (last bead of MT) and the closest bead on the KT surface. Each MT plus end is undergoing a stochastic dynamic instability process determined by four parameters: growth and shortening rates, and catastrophe and rescue frequencies.

Chemical components

The SRDDM has the following *chemically active* components: phosphatase and Aurora B kinase, Ndc80 linkers, and chromokinesin motors (Table 1 and Figure 1; see also Supplemental Tables S1 and S2). The chemical reactions, MT dynamic processes, and all of their rate constants, are listed in Supplemental Table S1, which also shows the transport properties (diffusion) of Aurora B. A bead-spring representation was also implemented to model CK, existing on the surface of a CH arm, such that when an MT is at a sufficiently close distance to the CH, a linkage is formed where one of the harmonically coupled beads is on the surface of the CH arm, and the other bead is on the surface of the MT (see Supplemental Eq. S8). The cell boundary of an ellipsoidal shape (Figure 1) delineates the interior space of the cell (Supplemental Eq. S10), which contains the uniformly distributed components, such as the phosphatase, as well as components localized to specific locations inside the cell, including Aurora B kinase.

Mechanochemistry

The SRDDM describes the following mechanochemical aspects: formation of the reversible noncovalent bonds between the MT plus ends and KT corona surface, and between the MT and CH arms, which facilitates the application of pulling and pushing forces by the MT (Table 1 and Figure 1; see also Supplemental Tables S1 and S2). For example, in addition to the polymerization and depolymerization dynamics, MTs are capable of forming noncovalent bonds with the KTs' surface via Ndc80 linkers and with CH arms via CK motors. The Ndc80 linkers are modeled implicitly as harmonic springs between the plus end of an MT and the KT corona surface (see Supplemental Eq. S7). CKs are defined explicitly as harmonic springs: when a CK attachment reaction occurs (Supplemental Table S1), one of the harmonically coupled beads is placed on the surface of the MT cylinder, and the other bead is placed on the surface of the CH arm cylinder. The kinetics of MTs, Ndc80 linkers, and CK motors are described using the reaction–diffusion master equation (RDME; Supplemental Eq. S1); the mechanics of MTs, Ndc80s, and CKs are described using the LD (Supplemental Eqs. S7, S8, and S14–S17). After their detachment (see Supplemental Table S1), the Ndc80 linker and CK motor do not have any mechanical impact.

Force field and equations of motion for mechanical components

To describe the force-generating and force-dependent processes, we introduce the mechanical energies and forces for the mechanically active components, for the noncovalent bonds they form, and for their interactions with the cell boundary. The mechanically active components are listed in Table 1 and are graphically illustrated in Figure 1. All the potential energy functions (force field) and the force-field parameters for all these components are described in detail in the SM (see Supplemental Eqs. S2–S10 and Supplemental Table S2). We describe MTs and CH arms using cylinder representation. The effect of excluded volume interaction between any two particles is also considered. Mathematical formulas for the mechanical energies and excluded volume interactions are given in the SM (Supplemental Eq. S2). We used LD formalism to describe the mechanical coupling and force generation and transduction, for example, to compute deformations and movements of all the mechanical components (see Supplemental Eqs. S14–S17). The cell dynamic mechanical evolution is simulated by propagating the Langevin equations of motion forward in time in the overdamped (Brownian diffusion) limit for each mechanical component. Further information and mathematical details are described in the SM.

Chemical reactions and molecular transport

We used a numerical implementation of the RDME approach (Gardiner *et al.*, 1976; Isaacson, 2009; Isaacson and Isaacson, 2009) to model the biochemical reactions that involve chemically active components and molecular transport (diffusion; see the SM for more details; Supplemental Eq. S1). In the RDME approach, all the chemical interactions are described based upon the propensities of

chemical reactions (Gillespie, 1976, 1977). In our implementation, the cell volume is divided into a large number of small subcells (see Supplemental Table S2). The molecules within the cell are distributed among subcells. Chemical reactions are allowed between molecules within a subcell, and the molecules can diffuse randomly between the next-neighbor subcells (see Supplemental Table S1).

Model implementation

The SRDDM was mapped into the CellDynaMo package implemented on graphics processing units. We used the next-subvolume method extension (Elf and Ehrenberg, 2004) of the original Gillespie algorithm (Gillespie, 1976, 1977) in conjunction with the multiparticle diffusion approach (Roberts *et al.*, 2013). Numerical routines for the generation of (pseudo)random numbers (Hybrid Taus), and for RDME and LD are described elsewhere (Zhmurov et al., 2010, 2011).

ACKNOWLEDGMENTS

V.B. acknowledges the support from National Institutes of Health (Grant no. R01HL-148227) and from National Science Foundation (Grant no. MCB-2027530). A.M. acknowledges the support from National Science Foundation (Grant no. DMS1953430).

REFERENCES

Akiyoshi B, Sarangapani KK, Powers AF, Nelson CR, Reichow SL, Arellano-Santoyo H, Gonen T, Ranish JA, Asbury CL, Biggins S (2010). Tension directly stabilizes reconstituted kinetochore-microtubule attachments. Nature 468, 576–579.

Almeida AC, Maiato H (2018). Chromokinesins. Curr Biol 28, R1131–R1135.

Baudoin NC, Nicholson JM, Soto K, Martin O, Chen J, Cimini D (2020). Asymmetric clustering of centrosomes defines the early evolution of tetraploid cells. Elife 9, e54565.

Bentovim L, Harden TT, DePace AH (2017). Transcriptional precision and accuracy in development: from measurements to models and mechanisms. Development 144, 3855–3866.

Blackwell R, *et al.* (2017). Contributions of microtubule dynamic instability and rotational diffusion to kinetochore capture. Biophys J 112, 552–563.

Brouhard GJ, Hunt AJ (2005). Microtubule movements on the arms of mitotic chromosomes: polar ejection forces quantified in vitro. Proc Natl Acad Sci USA 102, 13903–13908.

Cane S, Ye AA, Luks-Morgan SJ, Maresca TJ (2013). Elevated polar ejection forces stabilize kinetochore-microtubule attachments. J Cell Biol 200, 203–218.

Cimini D (2008). Merotelic kinetochore orientation, aneuploidy, and cancer. Biochim Biophys Acta Rev Cancer 1786, 32–40.

Cimini D, Cameron LA, Salmon ED (2004). Anaphase spindle mechanics prevent mis-segregation of merotelically oriented chromosomes. Artif Intell Med 14, 2149–2155.

Cimini D, Degrassi F (2005). Aneuploidy: a matter of bad connections. Trends Cell Biol 15, 442–451.

Cimini D, Moree B, Canman JC, Salmon ED (2003). Merotelic kinetochore orientation occurs frequently during early mitosis in mammalian tissue cells and error correction is achieved by two different mechanisms. J Cell Sci 116, 4213–4225.

Cimini D, Wan X, Hirel CB, Salmon ED (2006). Aurora kinase promotes turnover of kinetochore microtubules to reduce chromosome segregation errors. Curr Biol 16, 1711–1718.

Conti D, Gul P, Islam A, Martín-Durán JM, Pickersgill RW, Draviam VM (2019). Kinetochores attached to microtubule-ends are stabilised by Astrin bound PP1 to ensure proper chromosome segregation. Elife 8, e49325.

Drake T, Vavylonis D (2010). Cytoskeletal dynamics in fission yeast: a review of models for polarization and division. HFSP J 4, 122–130.

Drpic D, Almeida AC, Aguiar P, Renda F, Damas J, Lewin HA, Larkin DM, Khodjakov A, Maiato H (2018). Chromosome segregation is biased by kinetochore size. Curr Biol 28, 1344–1356.

Edelmaier CJ, Lamson AR, Gergely ZR, Ansari S, Blackwell R, Richard McIntosh J, Glaser, MA, Betterton MD (2020). Mechanisms of chromosome biorientation and bipolar spindle assembly analyzed by computational modeling. Elife 9, 1–48.

Elf J, Ehrenberg M (2004). Spontaneous separation of bi-stable biochemical systems into spatial domains of opposite phases. Syst Biol (Stevenage) 1, 230–236.

Farhadifar R, Yu C-H, Fabig G, Wu H-Y, Stein DB, Rockman M, Müller-Reichert T, Shelley MJ, Needleman DJ (2020). Stoichiometric interactions explain spindle dynamics and scaling across 100 million years of nematode evolution. Elife 9, e55877.

Gardiner CW, McNeil KJ, Walls DF, Matheson IS (1976). Correlations in stochastic theories of chemical reactions. J Stat Phys 14, 307–331.

Gay G, Courtheoux T, Reyes C, Tournier S, Gachet Y (2012). A stochastic model of kinetochore-microtubule attachment accurately describes fission yeast chromosome segregation. J Cell Biol 196, 757–774.

Gillespie DT (1976). A general method for numerically simulating coupled chemical reactions. J Comput Phys 22, 403–434.

Gillespie DT (1977). Exact stochastic simulation of coupled chemical reactions. J Phys Chem 81, 2340–2361.

Gopalakrishnan M, Govindan BS (2011). A first-passage-time theory for search and capture of chromosomes by microtubules in mitosis. Bull Math Biol 73, 2483–2506.

Gregan J, Polakova S, Zhang L, Tolić-Nørrelykke IM, Cimini D (2011). Merotelic kinetochore attachment: causes and effects. Trends Cell Biol 21, 374–381.

Gundersen GG (2002). Evolutionary conservation of microtubule-capture mechanisms. Nat Rev Mol Cell Biol 3, 296–304.

Heald R, Khodjakov A (2015). Thirty years of search and capture: the complex simplicity of mitotic spindle assembly. J Cell Biol 211, 1103–1111.

Hill TL (1985). Theoretical problems related to the attachment of microtubules to kinetochores. Proc Natl Acad Sci USA 82, 4404–4408.

Holy TE, Leibler S (1994). Dynamic instability of microtubules as an efficient way to search in space. Proc Natl Acad Sci USA 91, 5682–5685.

Isaacson SA (2009). The reaction-diffusion master equation as an asymptotic approximation of diffusion to a small target. SIAM J Appl Math 70, 77–111.

Isaacson SA, Isaacson D (2009). Reaction-diffusion master equation, diffusion-limited reactions, and singular potentials. Phys Rev E - Stat Nonlinear, Soft Matter Phys 80, 1–9.

Kalinina I, Nandi A, Delivani P, Chacón MR, Klemm AH, Ramunno-Johnson D, Krull A, Lindner B, Pavin N, Tolić-Nørrelykke IM (2013). Pivoting of microtubules around the spindle pole accelerates kinetochore capture. Nat Cell Biol 15, 82–87.

Kirschner M, Mitchison T (1986). Beyond self-assembly: from microtubules to morphogenesis. Cell 45, 329–342.

Kliuchnikov E, Zhmurov A, Marx KA, Mogilner A, Barsegov V (2022). CellDynaMo–stochastic reaction-diffusion-dynamics model: application to search-and-capture process of mitotic spindle assembly. PLoS Comput Biol 18, e1010165.

Krenn V, Musacchio A (2015). The Aurora B kinase in chromosome bi-orientation and spindle checkpoint signaling. Front Oncol 5, 225.

Lampson MA, Cheeseman IM (2011). Sensing centromere tension: Aurora B and the regulation of kinetochore function. Trends Cell Biol 21, 133–140.

Lampson MA, Grishchuk EL (2017). Mechanisms to avoid and correct erroneous kinetochore-microtubule attachments. Biology (Basel) 6, 1.

Lee L, Tirnauer JS, Li J, Schuyler SC, Liu JY, Pellman D (2000). Positioning of the mitotic spindle by a cortical-microtubule capture mechanism. Science 287, 2260–2262.

Letort G, Bennabi I, Dmitrieff S, Nedelec F, Verlhac M-H, Terret M-E (2019). A computational model of the early stages of acentriolar meiotic spindle assembly. Mol Biol Cell 30, 863–875.

Li X, Bloomfield M, Bridgeland A, Cimini D, Chen J (2022). How a cell achieves bipolar spindle assembly with normal or aberrant centrosome numbers. Biophys J 121, 122a.

Liu D, Vader G, Vromans MJM, Lampson MA, Lens SMA (2009). Sensing chromosome bi-orientation kinase from kinetochore substrates. Science 323, 1350–1353.

Magidson V, O'Connell CB, Lončarek J, Paul R, Mogilner A, Khodjakov A (2011). The spatial arrangement of chromosomes during prometaphase facilitates spindle assembly. Cell 146, 555–567.

Magidson V, Paul R, Yang N, Ault JG, O'Connell CB, Tikhonenko I, Mcewen BF, Mogilner A, Khodjakov A (2015). Adaptive changes in the kinetochore architecture facilitate proper spindle assembly. Nat Cell Biol 17, 1134–1144.

Maresca TJ, Salmon ED (2009). Intrakinetochore stretch is associated with changes in kinetochore phosphorylation and spindle assembly checkpoint activity. J Cell Biol 184, 373–381.

Meunier S, Vernos I (2016). Acentrosomal microtubule assembly in mitosis: the where, when, and how. Trends Cell Biol 26, 80–87.

Nédélec F (2002). Computer simulations reveal motor properties generating stable antiparallel microtubule interactions. J Cell Biol 158, 1005–1015.
Nicklas RB (1997). How cells get the right chromosomes. Science 275, 632–637.
Nicklas RB, Koch CA (1969). Chromosome micromanipulations: III. spindle fiber tension and the reorientation of mal-oriented chromosomes. J Cell Biol 43, 40–50.
Nicklas RB, Ward SC (1994). Elements of error correction in mitosis: microtubule capture, release, and tension. J Cell Biol 126, 1241–1253.
O'Connell CB, Khodjakov AL (2007). Cooperative mechanisms of mitotic spindle formation. J Cell Sci 120, 1717–1722.
Ostergren G (1951). The mechanism of co-orientation in bivalents and multivalents. Hereditas 37, 85–156.
Paul R, Wollman R, Silkworth WT, Nardi IK, Cimini D, Mogilner A (2009). Computer simulations predict that chromosome movements and rotations accelerate mitotic spindle assembly without compromising accuracy. Proc Natl Acad Sci USA 106, 15708–15713.
Pavin N, Tolić IM (2016). Self-organization and forces in the mitotic spindle. Annu Rev Biophys 45, 279–298.
Peterman EJG, Scholey JM (2009). Mitotic microtubule crosslinkers: insights from mechanistic studies. Curr Biol 19, R1089–R1094.
Renda F, Miles C, Tikhonenko I, Fisher R, Carlini L, Kapoor TM, Mogilner A, Khodjakov A (2022). Non-centrosomal microtubules at kinetochores promote rapid chromosome biorientation during mitosis in human cells. Curr Biol 32, 1049–1063.
Rieder CL, Alexander SP (1990). Kinetochores are transported poleward along a single astral microtubule during chromosome attachment to the spindle in newt lung cells. J Cell Biol 110, 81–95.
Roberts E, Stone JE, Luthey-Schulten Z (2013). Lattice microbes: high-performance stochastic simulation method for the reaction-diffusion master equation. J Comput Chem 34, 245–255.
Saka Y, Giuraniuc CV, Ohkura H (2015). Accurate chromosome segregation by probabilistic self-organisation. BMC Biol 13, 1–10.
Santaguida S, Amon A (2015). Short- and long-term effects of chromosome mis-segregation and aneuploidy. Nat Rev Mol Cell Biol 16, 473–485.
Sarkar A, Rieger H, Paul R (2019). Search and capture efficiency of dynamic microtubules for centrosome relocation during IS formation. Biophys J 116, 2079–2091.
Sikirzhytski V, Renda F, Tikhonenko I, Magidson V, McEwen BF, Khodjakov A (2018). Microtubules assemble near most kinetochores during early prometaphase in human cells. J Cell Biol 217, 2647–2659.
Silk AD, Zasadil LM, Holland AJ, Vitre B, Cleveland DW, Weaver BA (2013). Chromosome missegregation rate predicts whether aneuploidy will promote or suppress tumors. Proc Natl Acad Sci USA 110, E4134–E4141.
Silkworth WT, Nardi IK, Paul R, Mogilner A, Cimini D (2012). Timing of centrosome separation is important for accurate chromosome segregation. Mol Biol Cell 23, 401–411.
Thawani A, Stone HA, Shaevitz JW, Petry S (2019). Spatiotemporal organization of branched microtubule networks. Elife 8, e43890.
Tubman ES, Biggins S, Odde DJ (2017). Stochastic modeling yields a mechanistic framework for spindle attachment error correction in budding yeast mitosis. Cell Syst 4, 645–650.
Vaisberg EA, Koonce MP, McIntosh JR (1993). Cytoplasmic dynein plays a role in mammalian mitotic spindle formation. J Cell Biol 123, 849–858.
Vinogradova T, Paul R, Grimaldi AD, Loncarek J, Miller PM, Yampolsky D, Magidson V, Khodjakov A, Mogilner A, Kaverina I (2012). Concerted effort of centrosomal and Golgi-derived microtubules is required for proper Golgi complex assembly but not for maintenance. Mol Biol Cell 23, 820–833.
Wollman R, Cytrynbaum EN, Jones JT, Meyer T, Scholey JM, Mogilner A (2005). Efficient chromosome capture requires a bias in the "search-and-capture" process during mitotic-spindle assembly. Curr Biol 15, 828–832.
Ye AA, Cane S, Maresca TJ (2016). Chromosome biorientation produces hundreds of piconewtons at a metazoan kinetochore. Nat Commun 7, 1–9.
Zaytsev AV, Grishchuk EL (2015). Basic mechanism for biorientation of mitotic chromosomes is provided by the kinetochore geometry and indiscriminate turnover of kinetochore microtubules. Mol Biol Cell 26, 3985–3998.
Zhmurov A, Rybnikov K, Kholodov Y, Barsegov V (2010). Efficient pseudo-random number generators for biomolecular simulations on graphics processors. ArXiv preprint arxiv:10031123.
Zhmurov A, Rybnikov K, Kholodov Y, Barsegov V (2011). Generation of random numbers on graphics processors: forced indentation *in silico* of the bacteriophage HK97. J Phys Chem B 115, 5278–5288.